Tropical chemical weathering of hillslope deposits and bedrock source in the Aburrá Valley, northern Colombian Andes

Article *in* Engineering Geology · November 2005

DOI: 10.1016/j.enggeo.2005.08.001

CITATIONS
62

READS
1,365

3 authors, including:

Edier Aristizábal
Universität Potsdam
86 PUBLICATIONS **673** CITATIONS

SEE PROFILE

Available online at www.sciencedirect.com
SCIENCE DIRECT
ELSEVIER
Engineering Geology 81 (2005) 389–406
ENGINEERING GEOLOGY
www.elsevier.com/locate/enggeo

Tropical chemical weathering of hillslope deposits and bedrock source in the Aburrá Valley, northern Colombian Andes

Edier Aristizábal [1], Barry Roser *, Shuichiro Yokota

Department of Geoscience, Shimane University, Matsue 690-8504, Japan

Received 3 June 2005; received in revised form 28 July 2005; accepted 13 August 2005
Available online 3 October 2005

Abstract

Tropical chemical weathering produces extensive lateritization and formation of deep weathering profiles. Both processes are fundamental to landscape evolution and slope instability. The Aburrá Valley of the northern Colombian Andes is characterized by tropical conditions. The valley slopes are mostly covered by hillslope deposits originating from four basement rock suites which comprise contrasting granitoid, volcanic–sedimentary, ophiolitic, and metamorphic sources, respectively. Tropical chemical weathering of the Aburrá hillslope deposits and their respective bedrock were examined using X-ray fluorescence and X-ray diffraction analysis, to document and quantify their chemical weathering profiles, compositions, and mineralogical properties. The Chemical Index of Alteration (CIA), loss on ignition (LOI), and the Mobiles index (Imob) were used to quantify the degree of weathering of hillslope deposits and bedrock source. Weathering trends were analyzed using A–CN–K and A–CNK–FM diagrams. The material mantling the slopes in the Aburrá Valley records an intense weathering history. Chemical weathering is characterized by increased development of clay minerals (kaolinite, halloysite) and iron and aluminum sesquioxides. Lateritization characterizes the final stage of the weathering profiles. Concentrations of CaO, Na_2O, K_2O decrease markedly in the weathering products compared to the fresh bedrock source, whereas concentrations of Al_2O_3, Fe_2O_3, and MgO increase significantly. CIA ratios of matrix slope deposits derived from all four sources near 100, whereas those of boulder slope deposits and saprolites are lower, but exceed source rock values. Different A–CN–K weathering paths are evident for each lithotype, validating the correlation established between the hillslope deposits and their various parents. Chemical weathering indices in some samples are strongly influenced by the presence of sesquioxides, as reflected by high LOI, anomalously low CIA, and varying enrichment trends on the A–CNK–FM diagrams. Consequently, different chemical indices based on different criteria need to be combined to obtain best results, as illustrated here by the combination of LOI, CIA, and Imob. The overall results suggest that tropical conditions have dominated for a long time in the northern Colombian Andes, leading to uniformly high weathering indices in matrix slope deposits irrespective of parent lithotype. Prolonged warm and humid conditions could thus be responsible for the weathering and remobilization of extensive old hillslope deposits during the Quaternary. However, in addition to the influence of climatic factors, tectonism has also undoubtedly influenced slope evolution in the Aburrá Valley.

Keywords: Geochemistry; Tropical weathering; Weathering indices; Hillslope deposits; Colombia

1. Introduction

Chemical weathering is a dominant process in tropical regions, favoring extensive lateritization and formation of deeply weathered profiles (Irfan, 1996; Voicu

* Corresponding author. Fax: +81 852 326469.
E-mail address: roser@riko.shimane-u.ac.jp (B. Roser).
[1] Present address: Disaster Prevention Coordinator, Environmental Department, Aburrá Valley Metropolitan Area, Calle 41 No 53-07, Medellín, Colombia.

0013-7952/$ - see front matter © 2005 Elsevier B.V. All rights reserved.
doi:10.1016/j.enggeo.2005.08.001

and Bardoux, 2002). Weathering modifies the engineering properties of materials and may promote slope instability, as landslides often occur in areas strongly affected by weathering (Yokota and Iwamatsu, 1999; Ng et al., 2001; Arel and Tugrul, 2001; Rahardjo et al., 2004; Moon and Jayawardane, 2004).

Chemical weathering indices using quantitative measures based on whole-rock chemical analyses are commonly used for characterizing the intensity and mechanisms of weathering (Nesbitt and Young, 1982; Irfan, 1996, 1999; Ng et al., 2001; Gupta and Rao, 2001; Voicu and Bardoux, 2002). Recent work has shown that weathering indices based on the ratio of a group of mobile oxides to one or more immobile oxides are useful parameters for characterizing changes induced by weathering (Duzgoren-Aydin et al., 2002). Those elements that are most mobile during weathering are most effective in quantifying the effects of chemical weathering on heterogeneous weathering residua (Price and Velbel, 2003).

Nesbitt and Young (1982, 1984, 1989) and Nesbitt et al. (1996) used ternary A–CN–K and A–CNK–FM diagrams to deduce weathering trends. These authors demonstrated that the bulk compositions of diverse composition rocks follow simple trends that are largely unaffected by the climatic conditions under which weathering took place. In addition to providing a method of visualizing the degree of weathering, the A–CN–K system permits evaluation of the weathering trends from fresh rock compositions through to their weathering products (Fedo et al., 1995).

Most workers studying tropical weathering have concentrated on the geochemical and geomechanical changes in weathering profiles developed over bedrocks. However, some authors have also attempted to correlate weathering processes and hillslope deposits (McFadden, 1988; Modenesi-Gauttieri and de Toledo, 1996). The geomorphological evolution of the northern Colombian Andes corresponds to a natural input system strongly controlled by intensive weathering mechanisms and the generation of hillslope deposits. The Aburrá Valley of Colombia is a montane valley influenced by tropical climate conditions. Residual soils and hillslope deposits occupy most of the valley slopes. Both the ancient and recent history of the valley has been characterized by numerous occurrences of landslides, some of which have led to significant loss of life and substantial economic impacts.

The main objectives of this study were to study weathering trends and weathering intensity, chemical behavior of major elements, and mineralogy of hillslope deposits in the Aburrá Valley in relation to their parent rock type. Weathering characterization of parent rock and hillslope deposits is an essential tool to develop models linking tropical weathering processes and the instability condition of slopes. Additionally, it will provide valuable background information for reconstruction of the Quaternary landscape evolution of the Colombian Andes, and for understanding the role played by paleoclimatic conditions in that evolution.

2. Study area

The Colombian Andes are divided into three ranges: ancient and modern fold-thrust belts, named the Central and Oriental Cordillera, respectively; and an accreted arc known as the Occidental Cordillera (Cooper et al., 1995). The Aburrá Valley is located in the northern part of the Central Cordillera, approximately between latitudes 6°00′N to 6°30′N and longitudes 75°15′W to 75°45′W.

Weathering conditions in the Aburrá Valley are those of tropical zones. Temperatures vary little throughout the year, with annual average temperature of 22 °C, and mean relative humidity of 70% (PNUD-Medellín, 1995). Rainfall over the year is distinctly bimodal, with maximum precipitation in April/May and in October/November. Annual rainfall varies from 1400 mm in the central part of the valley to 2700 mm in the northern and southern parts.

3. Geological and geomorphological setting

The northern Central Cordillera of Colombia is composed of five complex geological units (Fig. 1): (1) Paleozoic metamorphic basement; (2) ultrabasic igneous rocks; (3) a volcano-sedimentary sequence; (4) intrusive granitoid bodies; and (5) hillslope deposits and alluvial sediments (Maya and Gonzalez, 1995). The metamorphic basement along the Aburrá Valley consists of amphibolites and gneisses, which crop out in the north, west and southeast. Dunites, gabbros, basalts, and sediments of oceanic origin, now strongly tectonized, were thrust over the metamorphic basement during Cretaceous times (Restrepo and Toussaint, 1984). Elongate bodies of these rocks oriented NW–SE crop out in the southwest and central parts of the Aburrá Valley. Acid to intermediate Triassic and Cretaceous plutonic bodies (tonalities and granodiorites) intrude the metamorphic belt (McCourt et al., 1984; Kerr et al., 1996), and crop out in the north and west.

The region has been tectonically active for millions of years (GSM, 2002; Rendón, 2003). Structural trends

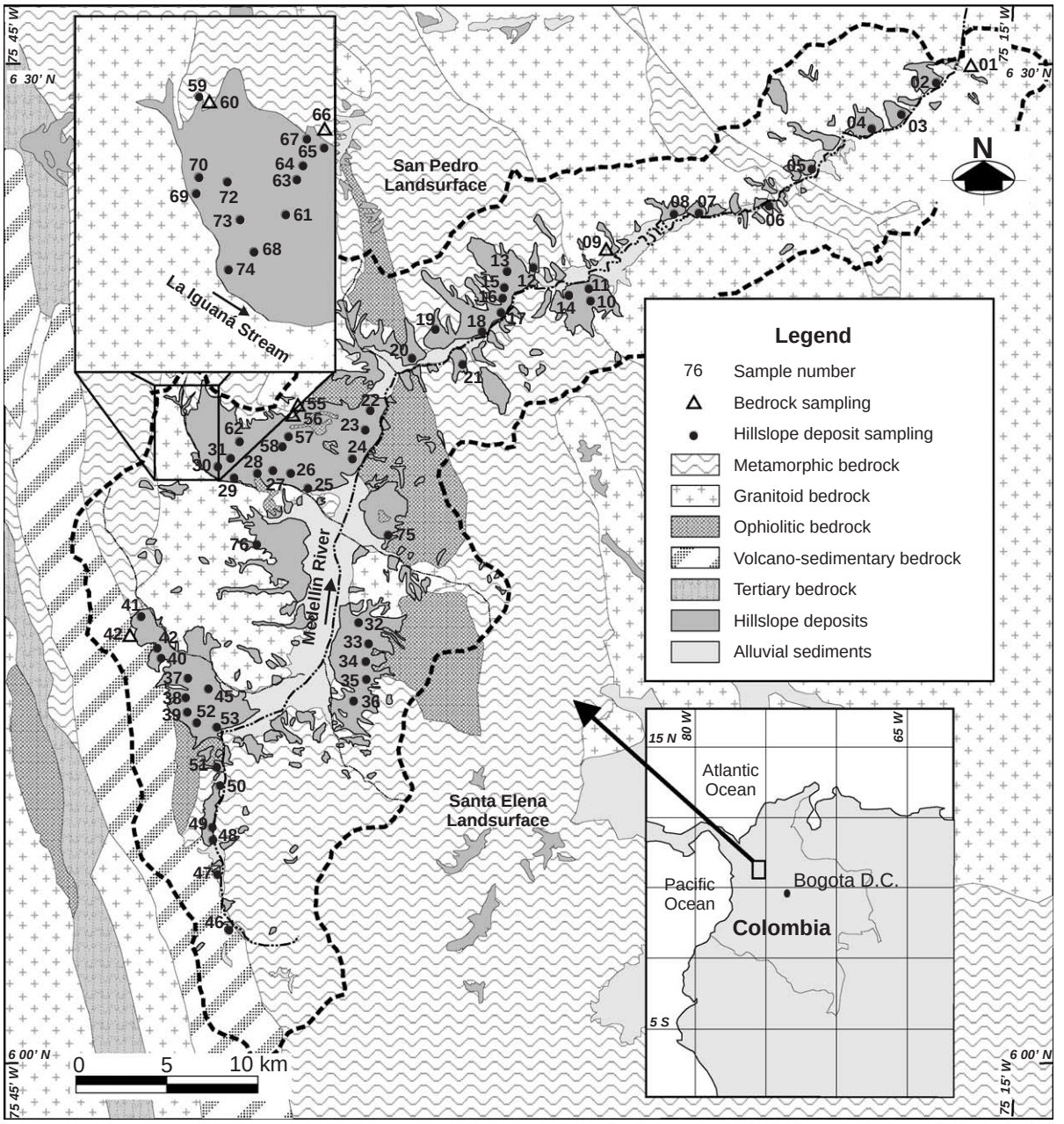

Fig. 1. Simplified geological map of the Aburrá Valley and hillslope deposit and bedrock sample locations. The dotted line marks the border of the catchment. Inset at upper left: detailed sampling in the Iguana Stream valley; lower right: location in Colombia.

related to tectonic evolution of the Aburrá Valley are represented by the Romeral Fault System, with regional evidence of both right-lateral and left-lateral slip (Ego and Sebrier, 1995). The most dominant and persistent fault directions trend NNW–SSE. Drainage anomalies and shear zones have also been reported, reflecting recent tectonic movements along subordinate fault structures (GSM, 2002; Rendón, 2003; Yokota and Ortiz, 2003).

The Aburrá Valley can be divided into three broad geomorphologic sectors. The central portion consists of broad alluvial plains bounded by moderate to gentle slopes; whereas the northern and southern parts consist of narrow asymmetric valleys bounded by steep slopes. Older erosion features known as the Santa Elena (2750 m a.s.l). and the San Pedro (2800 m a.s.l.) land surfaces flank the valley to the north and the east, but are absent in the southwestern sector.

Bedrock surfaces and steep-sloped hills crop out on the upper valley slopes. Thick deposits ranging from late Pliocene to Holocene in age cover the lower and middle slopes (Restrepo, 1991; Yokota and Ortiz, 2003; Rendón, 2003). They are mixtures derived from multiple mass movements, mainly debris flows and debris slides. The deposits are massive in texture and are poorly sorted. The matrix is silty clay, reddish-brown to orange-brown, supporting mixtures of angular fragments ranging in size from cobbles through to boulders meters in diameter.

The slopes of the Aburrá Valley are overlain by a thick weathering profile. Depths of weathering profiles vary significantly depending on parent rock lithology and local conditions. They are thicker on gentle slopes, and decrease in thickness on steep slopes due to erosion. On the granitoids, weathering profiles consist of deep yellowish-red (10YR 7/4) residual soils and saprolites over 50 m thick overlying up to 100 m of weathered and disintegrated rock. The boundaries between weathered rocks and saprolites are extremely irregular and difficult to recognize, because they are strongly controlled by groundwater movement and networks of joints. The weathering profiles developed on the ultrabasic and metamorphic rocks are thinner, varying between 50 and 80 m in thickness. They are generally reddish orange (7.5 YR 7/6), and contain highly weathered rock fragments.

4. Materials and methods

Almost one hundred samples were collected from the Aburrá Valley (Fig. 1). The samples include matrix and boulders from hillslope deposits, and fresh rock and saprolites from bedrock sources. Sampling was made according to the distribution of the hillslope deposits and bedrock sources. Matrix and boulder samples were collected from hillslope deposits along the entire course of the Aburrá Valley, in an attempt to fully represent the material present. Fresh rock and saprolites were also collected from the four main geological units which crop out in the valley, as close as possible to the areas from which the hillslope deposits were generated. The samples were then grouped by source, to compare the weathered material that forms the hillslope deposits with the bedrock from which they were derived. The samples were thus divided into four suites according to source lithotype: (1) granitoid source, (2) volcanic–sedimentary source, (3) ophiolitic source; and (4) metamorphic source.

X-ray fluorescence (XRF) and X-ray diffraction (XRD) analysis were used to document and quantify the chemical weathering profiles, compositions, and mineralogical properties of bedrocks and hillslope deposits in the Aburrá Valley. Bulk samples were first powdered by hand in an agate mill and dried at 60 °C for 12 h at the soil laboratory of the Universidad Nacional de Colombia (Medellín). Subsequent sample preparation and all analyses were carried out in the Department of Geoscience, Shimane University. The procedure for the preparation of samples is described by Roser et al. (1998).

Loss on ignition (LOI) was determined by ignition of samples in ceramic crucibles at 1050 °C for 2 h. Major element analyses were obtained using a Rigaku RIX-2000 spectrometer equipped with an Rh-anode X-ray tube. The analyses were made on glass beads prepared using an alkali flux comprising 80% lithium tetraborate and 20% lithium metaborate, sample weight of 1.8 g, and a sample to flux ratio of 1:2. Analytical methods, instrumental conditions, and calibration methods used were those described by Kimura and Yamada (1996).

Bulk mineral compositions were determined by X-ray diffraction analysis (XRD). Step-scan powder diffraction data were collected using a Rigaku RINT automated X-ray powder diffractometer with a Bragg–Brentano goniometer equipped with incident and diffracted-beam soller slits, 1° divergence and anti-scatter slits, a 0.15 mm receiving slit, and a curve graphite diffracted-beam monochrometer. The normal-focus Cu X-ray tube was operated at 30 kV and 20 mA. Profiles were taken between 2° and 40° 2θ at a step interval of 0.04°2θ.

5. Bulk compositions of hillslope deposits and bedrocks

XRF major element results are given in Table 1, listed on an as-analyzed (ignited) basis, and differentiated by bedrock source. LOI is also tabulated to permit recalculation on a hydrous basis. Selected major element–Al_2O_3 variation diagrams plotted on an anhydrous basis are given for each group in Fig. 2 (granitoid source), 3 (volcanic–sedimentary source), 4 (ophiolitic source), and 5 (metamorphic source). The elements plotted are the mobile species CaO, Na_2O, and K_2O, along with Fe_2O_3 (total iron as Fe_2O_3), as a representative of a less mobile element, although Fe abundances may also be influenced by sesquioxide development. The plots show general chemical fractionation between fresh and highly decomposed materials. The trends are formed by rock and saprolite source materials, followed successively by boulders and matrix slope deposits.

Table 1
Major element analyses of hillslope deposits and sources in the Aburrá Valley (anhydrous basis, wt.%)

SA#	Type	Lithology	SiO_2	TiO_2	Al_2O_3	Fe_2O_3	MnO	MgO	CaO	Na_2O	K_2O	P_2O_5	Total	CIA	LOI	I mob
Granitoid source																
M55B	R	Tonalite	64.57	0.52	16.76	4.72	0.11	1.71	5.21	3.61	1.67	0.15	99.64	50	0.59	0.00
M01	S	Tonalite	59.35	0.67	18.84	7.35	0.13	2.97	2.69	0.94	1.03	0.04	100.05	72	6.04	0.54
M09A	S	Tonalite	55.13	0.99	24.53	9.54	0.01	0.25	0.04	0.08	0.07	0.06	101.22	99	10.52	0.98
M09B	S	Tonalite	48.47	1.16	28.71	10.97	0.03	0.26	0.04	0.25	0.28	0.06	101.88	98	11.67	0.95
M09C	S	Tonalite	50.97	0.82	29.22	8.32	0.12	0.37	0.04	0.08	0.49	0.06	101.44	98	10.95	0.95
M09D	S	Tonalite	55.47	0.65	25.54	7.36	0.17	1.07	0.04	0.07	1.07	0.06	101.15	95	9.65	0.91
M55A	S	Tonalite	61.32	0.33	20.14	3.81	0.11	1.28	5.34	3.70	1.43	0.18	99.49	54	1.85	0.00
M02	M	Debris flow dep.	61.33	0.73	20.61	7.61	0.02	0.41	0.06	0.13	0.88	0.05	101.14	95	9.33	0.92
M03	M	Debris flow dep.	53.76	0.87	25.23	8.11	0.02	0.29	0.05	0.15	0.38	0.04	101.72	97	12.82	0.95
M07	M	Debris flow dep.	60.52	0.79	23.02	7.09	0.02	0.27	0.05	0.04	0.35	0.07	101.53	98	9.33	0.97
M08	M	Debris flow dep.	49.52	0.98	28.74	9.39	0.02	0.53	0.07	0.05	1.05	0.10	101.73	96	11.27	0.91
M76	M	Debris flow dep.	55.41	1.15	25.22	7.45	0.06	1.06	0.54	0.27	0.67	0.07	101.61	93	9.73	0.87
Volcanic–sedimentary source																
M42	R	Basalt	61.51	0.53	14.03	6.40	0.12	3.23	6.70	2.11	0.80	0.11	98.43	46	2.88	0.00
M37B	B	Basalt	49.62	0.72	18.25	10.74	0.09	5.27	6.58	2.48	0.08	0.09	100.04	53	6.12	0.01
M37A	M	Debris flow dep.	54.10	1.00	24.34	9.11	0.05	0.95	0.06	0.22	2.32	0.04	101.13	89	8.95	0.81
M38	M	Debris flow dep.	65.40	1.10	16.28	8.38	0.01	1.19	0.10	0.13	0.05	0.03	100.49	98	7.82	0.97
M39	M	Debris flow dep.	51.57	0.91	26.06	10.94	0.05	0.59	0.05	0.07	0.35	0.07	101.26	98	10.60	0.96
M40	M	Debris flow dep.	53.69	0.88	24.95	10.32	0.04	0.78	0.09	0.07	0.60	0.06	101.45	97	9.98	0.94
M41	M	Debris flow dep.	54.19	0.87	21.95	11.01	0.19	1.98	0.16	0.10	0.61	0.10	100.72	96	9.55	0.93
M44	M	Debris flow dep.	54.48	0.97	22.95	10.87	0.25	1.08	0.09	0.09	0.47	0.05	100.92	97	9.62	0.95
M45	M	Debris flow dep.	55.67	0.67	18.13	8.63	0.40	2.90	4.12	1.03	0.79	0.07	99.72	65	7.31	0.37
M48	M	Debris flow dep.	47.66	1.87	20.88	13.45	0.36	3.09	1.09	0.83	0.73	0.14	99.54	85	9.44	0.73
M49	M	Debris flow dep.	43.01	2.68	21.73	17.26	0.20	2.65	0.40	0.28	0.47	0.20	99.67	95	10.79	0.89
M50A	M	Alluviotorrential	50.28	1.10	25.93	9.39	0.15	1.19	0.32	0.12	0.39	0.09	101.15	96	12.20	0.92
M50B	M	Debris flow dep.	44.15	0.84	29.41	7.17	0.18	2.09	1.28	0.49	0.52	0.12	101.27	90	15.04	0.75
M50D	M	Alluviotorrential	53.66	0.83	20.77	9.57	0.17	2.71	2.93	0.61	1.06	0.11	100.35	74	7.93	0.53
M52	M	Debris flow dep.	49.08	0.97	25.66	11.65	0.19	1.20	0.11	0.09	1.74	0.14	101.13	93	10.29	0.86
M53	M	Debris flow dep.	47.13	1.03	28.40	11.51	0.01	0.54	0.10	0.12	0.51	0.06	101.20	97	11.81	0.94
Ophiolitic source																
M56B	R	Metagabbro	44.66	1.68	17.01	9.65	0.17	4.37	9.10	2.35	0.58	0.26	99.88	45	10.06	0.00
M56A	S	Metagabbro	46.24	1.22	28.05	7.26	0.13	1.51	5.85	1.54	0.87	0.62	101.00	69	7.72	0.35
M23B	B	Metagabbro	4.25	0.57	53.24	11.89	0.00	0.72	0.34	0.00	0.31	0.02	101.62	98	30.26	0.94
M24B	B	Metagabbro	24.82	1.80	18.27	22.03	2.71	0.64	0.04	0.21	0.25	0.11	99.04	98	28.15	0.96
M57B	B	Metagabbro	46.11	1.30	15.74	12.18	0.17	8.98	12.47	1.93	0.07	0.09	99.94	38	0.89	0.00
M75F	B	Metagabbro	48.98	0.48	16.43	7.54	0.13	9.14	12.59	2.33	0.11	0.02	99.33	38	1.60	0.00
M75W	B	Metagabbro	48.35	0.49	16.91	7.56	0.13	9.12	12.26	1.92	0.09	0.01	99.04	40	2.20	0.00
M22	M	Debris flow dep.	39.12	1.55	26.93	17.48	0.76	0.30	0.09	0.26	0.07	0.04	99.34	98	12.74	0.97
M23A	M	Debris flow dep.	41.63	1.72	30.65	13.12	0.04	0.30	0.08	0.73	0.02	0.02	101.34	96	13.03	0.93
M24A	M	Debris flow dep.	38.19	1.18	31.97	14.38	0.06	0.33	0.04	0.02	0.02	0.02	100.43	100	14.23	0.99
M57A	M	Debris flow dep.	46.74	0.89	24.87	9.86	0.08	4.57	3.27	0.29	0.09	0.03	100.55	79	9.86	0.69
M58	M	Debris flow dep.	43.85	3.04	18.49	17.74	0.21	3.62	4.19	0.62	0.04	0.22	99.52	69	7.50	0.60
M75A	M	Debris flow dep.	43.15	0.22	7.03	20.30	0.07	14.94	1.67	0.08	0.20	0.01	96.63	68	8.96	0.84
Metamorphic source																
M60	R	Amphibolite	53.87	1.29	13.80	10.05	0.16	6.42	10.39	2.74	0.06	0.10	99.39	37	0.53	0.00
M66A	R	Amphibolite	56.46	1.14	14.11	8.61	1.26	5.21	9.71	2.76	0.09	0.10	100.52	39	1.06	0.00
M66B	S	Amphibolite	40.08	2.40	25.83	15.16	0.08	2.66	1.88	0.42	0.25	0.04	99.99	86	11.18	0.78
M15A	B	Amphibolite	44.68	1.05	16.14	11.07	0.41	11.64	3.85	0.89	0.03	0.02	99.80	66	10.02	0.58
M20D	B	Amphibolite	14.00	5.44	24.20	35.78	0.12	0.42	0.05	0.00	0.28	0.26	96.91	98	16.36	0.98
M25B	B	Amphibolite	28.33	6.34	16.25	29.75	0.24	4.21	4.86	1.25	0.31	0.23	99.00	60	7.23	0.45
M29B	B	Amphibolite	48.50	1.61	14.41	11.99	0.19	7.77	10.79	1.98	0.05	0.11	99.44	39	2.04	0.00
M32B	B	Amphibolite	50.58	1.41	26.57	10.48	0.08	1.50	0.42	0.55	4.11	0.13	101.27	82	5.45	0.72
M33D	B	Amphibolite	49.24	0.22	17.74	6.23	0.11	8.98	12.74	2.02	0.08	0.01	98.92	40	1.54	0.00

(continued on next page)

Table 1 (*continued*)

SA#	Type	Lithology	SiO_2	TiO_2	Al_2O_3	Fe_2O_3	MnO	MgO	CaO	Na_2O	K_2O	P_2O_5	Total	CIA	LOI	I mob
M33F	B	Amphibolite	46.71	0.26	18.41	7.03	0.11	9.47	11.63	1.81	0.10	0.01	98.98	43	3.44	0.00
M69B	B	Amphibolite	40.22	1.84	18.40	14.34	0.17	8.08	9.68	0.87	0.04	0.07	100.25	9	6.54	0.09
M04	M	Debris flow dep.	56.06	0.78	26.08	7.35	0.04	0.28	0.05	0.00	0.18	0.06	101.15	99	10.32	0.99
M05	M	Debris flow dep.	61.58	0.68	20.37	6.40	0.10	1.10	0.16	0.26	1.64	0.12	100.54	90	8.13	0.88
M06	M	Debris flow dep.	62.10	0.69	19.77	6.32	0.10	1.07	0.15	0.15	1.68	0.11	100.08	91	7.95	0.89
M10	M	Debris flow dep.	33.79	2.47	30.04	18.42	0.04	0.27	0.06	0.09	0.00	0.04	99.51	99	14.30	0.99
M11	M	Debris flow dep.	39.60	1.81	28.15	16.59	0.14	0.51	0.06	0.16	0.19	0.12	99.78	99	12.45	0.97
M20A	M	Debris flow dep.	6.22	0.91	59.99	20.80	0.00	0.39	0.07	0.20	0.41	0.03	101.27	99	12.24	0.95
M20B	M	Debris flow dep.	32.81	1.58	23.19	25.54	0.08	2.82	0.08	0.13	0.23	0.04	99.28	98	12.77	0.97
M25A	M	Debris flow dep.	31.03	4.86	22.25	27.88	0.63	0.60	0.13	0.30	0.22	0.06	99.51	96	11.55	0.95
M33B	M	Debris flow dep.	25.45	0.21	9.08	42.07	0.09	5.89	0.49	0.37	0.27	0.05	95.22	85	11.25	0.90
M12	M	Debris flow dep.	39.04	3.75	25.75	17.95	0.15	0.51	0.10	0.20	0.02	0.11	99.82	99	12.23	0.97
M13	M	Debris flow dep.	43.11	1.90	27.92	13.64	0.19	0.51	0.08	0.46	0.04	0.03	100.16	97	12.27	0.95
M14	M	Debris flow dep.	39.50	2.27	27.93	14.73	0.15	1.78	0.85	0.66	0.08	0.05	100.86	92	12.87	0.86
M15B	M	Debris flow dep.	54.44	0.83	25.53	10.68	0.13	1.17	0.11	0.20	0.73	0.09	100.87	96	6.95	0.94
M16	M	Debris flow dep.	42.64	3.18	22.70	18.53	0.71	0.26	0.04	0.36	0.01	0.05	99.43	98	10.95	0.97
M17	M	Debris flow dep.	38.64	2.29	27.8	16.63	0.29	0.39	0.07	0.02	0.00	0.11	99.16	99	12.87	0.99
M18	M	Debris flow dep.	35.75	3.10	27.2	19.63	0.29	.29	0.07	0.10	0.00	0.10	99.18	100	12.74	0.99
M19	M	Debris flow dep.	46.08	1.67	21.34	13.88	0.21	3.91	3.33	0.58	0.06	0.02	99.89	75	8.81	0.65
M21	M	Debris flow dep.	48.26	1.82	18.26	11.52	0.16	6.00	6.59	1.04	0.03	0.03	99.57	57	5.85	0.35
M26	M	Debris flow dep.	37.65	2.39	28.37	17.48	0.06	0.31	0.10	0.20	0.00	0.06	99.60	99	12.98	0.97
M27	M	Debris flow dep.	38.62	2.24	29.28	15.54	0.04	0.36	0.07	0.18	0.00	0.07	99.33	99	12.94	0.98
M28A	M	Earth flow dep.	40.47	1.82	30.07	14.66	0.06	0.41	0.04	0.04	0.01	0.06	100.30	100	12.66	0.99
M28C	M	Debris flow dep.	41.17	2.16	29.91	13.79	0.15	0.33	0.04	0.08	0.02	0.06	100.48	100	12.78	0.99
M29A	M	Debris flow dep.	43.82	2.69	20.84	16.94	0.18	2.45	3.02	0.59	0.06	0.10	99.77	77	9.08	0.68
M30	M	Debris flow dep.	38.19	2.53	28.09	16.53	0.09	0.70	0.46	0.06	0.01	0.14	99.80	98	12.99	0.95
M31	M	Debris flow dep.	40.37	2.04	28.07	15.89	0.08	0.50	0.19	0.03	0.00	0.07	99.80	99	12.55	0.98
M32A	M	Debris flow dep.	56.52	1.17	22.62	7.05	0.08	1.55	0.79	0.82	1.20	0.06	99.62	85	7.74	0.80
M33A	M	Debris flow dep.	39.50	0.17	3.01	17.76	0.33	22.15	1.18	0.75	0.21	0.02	95.73	46	10.64	0.81
M34	M	Debris flow dep.	42.13	2.27	28.31	13.45	0.05	0.38	0.10	0.08	0.05	0.02	99.84	99	12.99	0.98
M35	M	Debris flow dep.	35.64	4.60	25.13	20.67	0.26	0.76	0.19	0.31	0.23	0.05	99.84	96	12.00	0.94
M36	M	Debris flow dep.	37.92	1.72	25.97	15.80	0.11	0.51	0.07	0.20	0.00	0.04	98.85	99	16.51	0.98
M46	M	Debris flow dep.	34.79	1.16	32.73	14.60	0.00	0.35	0.06	0.09	0.23	0.05	100.75	99	16.69	0.97
M47	M	Debris flow dep.	46.60	1.44	25.97	13.38	0.02	0.40	0.08	0.06	0.76	0.07	101.01	97	12.23	0.95
M51	M	Debris flow dep.	36.70	2.11	26.92	17.76	0.27	1.27	0.75	0.11	0.01	0.03	98.59	95	12.66	0.92
M59	M	Debris flow dep.	56.23	1.27	21.32	8.48	0.07	1.22	0.35	0.17	1.70	0.13	100.91	90	9.97	0.86
M61	M	Debris flow dep.	42.67	2.02	24.92	13.51	0.17	3.31	2.49	0.36	0.10	0.08	100.60	83	10.97	0.74
M62	M	Debris flow dep.	36.23	2.31	27.64	18.86	0.09	0.43	0.23	0.07	0.00	0.09	98.98	99	13.04	0.97
M63	M	Debris flow dep.	46.20	2.02	22.44	12.49	0.12	3.66	3.65	0.40	0.02	0.08	100.34	76	9.27	0.64
M64	M	Debris flow dep.	36.92	2.31	27.90	16.33	0.07	1.20	0.82	0.11	0.13	0.17	100.20	95	14.23	0.91
M65	M	Debris flow dep.	36.69	2.49	27.15	18.22	0.09	0.41	0.06	0.07	0.10	0.11	98.85	100	13.47	0.98
M67	M	Debris flow dep.	45.39	1.62	25.17	12.69	0.08	2.17	1.65	0.19	0.42	0.13	100.83	88	11.31	0.81
M68	M	Debris flow dep.	38.12	2.34	26.29	18.19	0.10	0.77	0.53	0.22	0.02	0.08	99.00	96	12.34	0.93
M69A	M	Debris flow dep.	37.52	2.33	30.22	14.03	0.06	0.51	0.09	0.07	0.20	0.07	100.12	99	15.01	0.97
M70	M	Debris flow dep.	36.03	1.97	27.44	13.80	0.09	0.42	0.12	0.07	0.07	0.07	99.46	99	19.38	0.98
M72	M	Debris flow dep.	51.88	1.42	22.92	10.63	0.09	1.30	0.46	0.34	1.07	0.09	101.08	91	10.88	0.87
M73	M	Debris flow dep.	36.66	2.55	27.96	17.79	0.17	0.70	0.14	0.03	0.03	0.09	99.19	100	13.05	0.98
M74	M	Debris flow dep.	44.67	1.58	28.79	12.19	0.06	0.56	0.15	0.07	0.14	0.05	100.54	99	12.27	0.97

Type—sample type; R—fresh bedrock; S—saprolite bedrock; B—boulder in slope deposits; M—Matrix in slope deposits. CIA—Chemical Index of Alteration; LOI—Loss on Ignition; Imob—Mobiles Index.

The weathering behavior of the oxides from fresh bedrock through to matrix material is generally characterized by enrichment in Al_2O_3, Fe_2O_3, and TiO_2, and depletion in CaO, Na_2O, K_2O, SiO_2, MgO, and MnO. Most samples from granitic and volcanic–sedimentary sources lie along linear trends (Figs. 2 and 3, respectively), whereas ophiolitic and metamorphic samples tend to scatter, especially for Fe_2O_3, CaO (Figs. 4 and 5), and MgO.

The oxide variation diagrams for granitoid sources (Fig. 2) show fresh protolith has an anhydrous Al_2O_3 content of 17%, whereas maximum values in the weathering products near 30 wt.%. TiO_2 (not illustrated) forms a linear trend which intersects the abscissa at

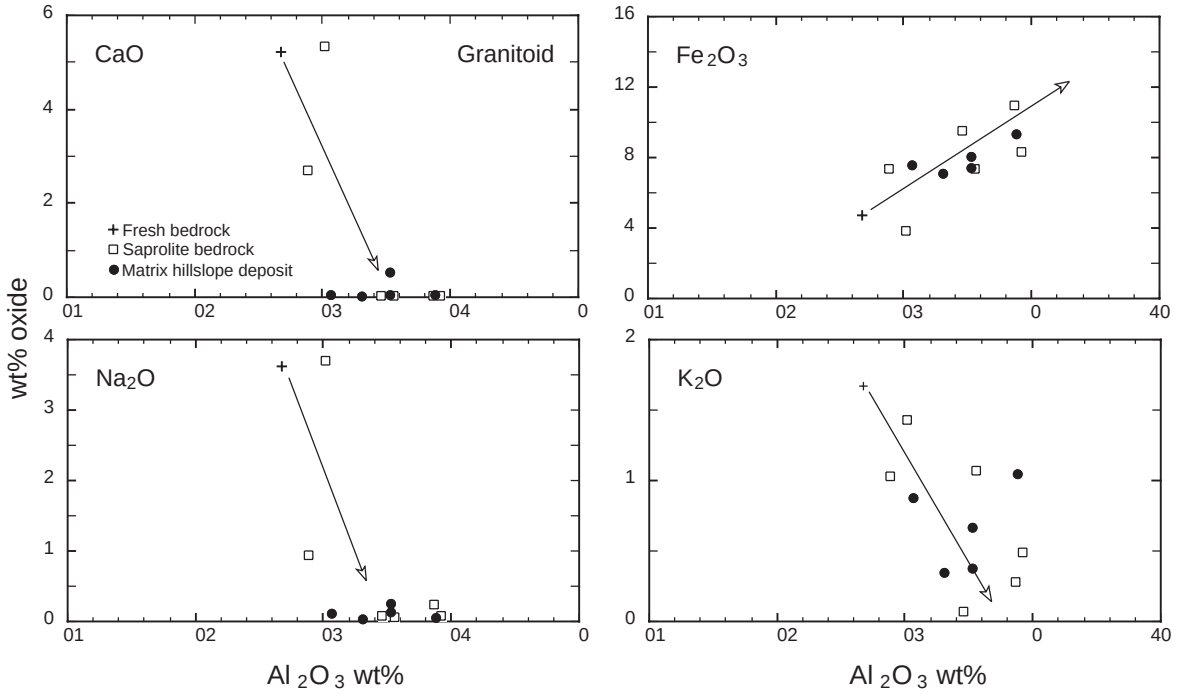

Fig. 2. Selected major element–Al_2O_3 variation diagrams (anhydrous basis) for samples derived from granitoid bedrock source. Arrows indicate general trends as weathering increases.

around 6% Al_2O_3. MnO and MgO (not illustrated) show weak negative correlation with Al_2O_3, ranging from 0.02 wt.% MnO and 0.25 wt.% MgO in weathered samples, to 0.1 wt.% MnO and 1.7 wt.% MgO in fresh samples, with a few samples scattering to higher values. SiO_2 abundances show broad negative correlation with

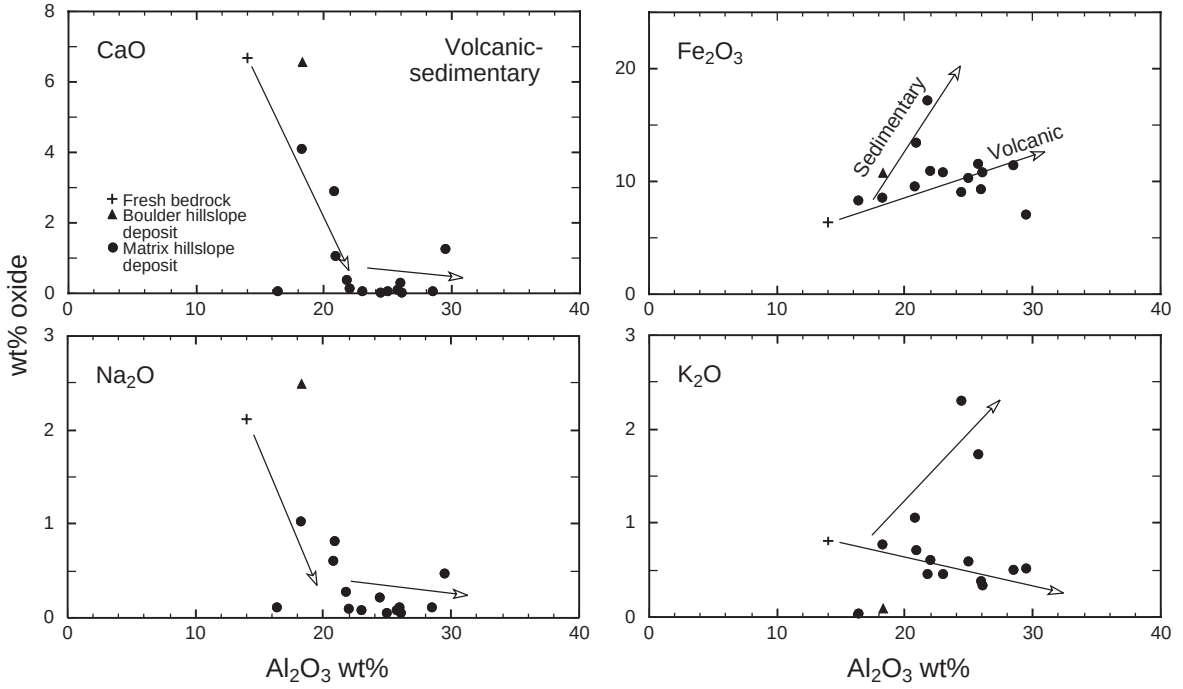

Fig. 3. Major element–Al_2O_3 variation diagrams (anhydrous basis) for samples derived from volcanic–sedimentary bedrock source.

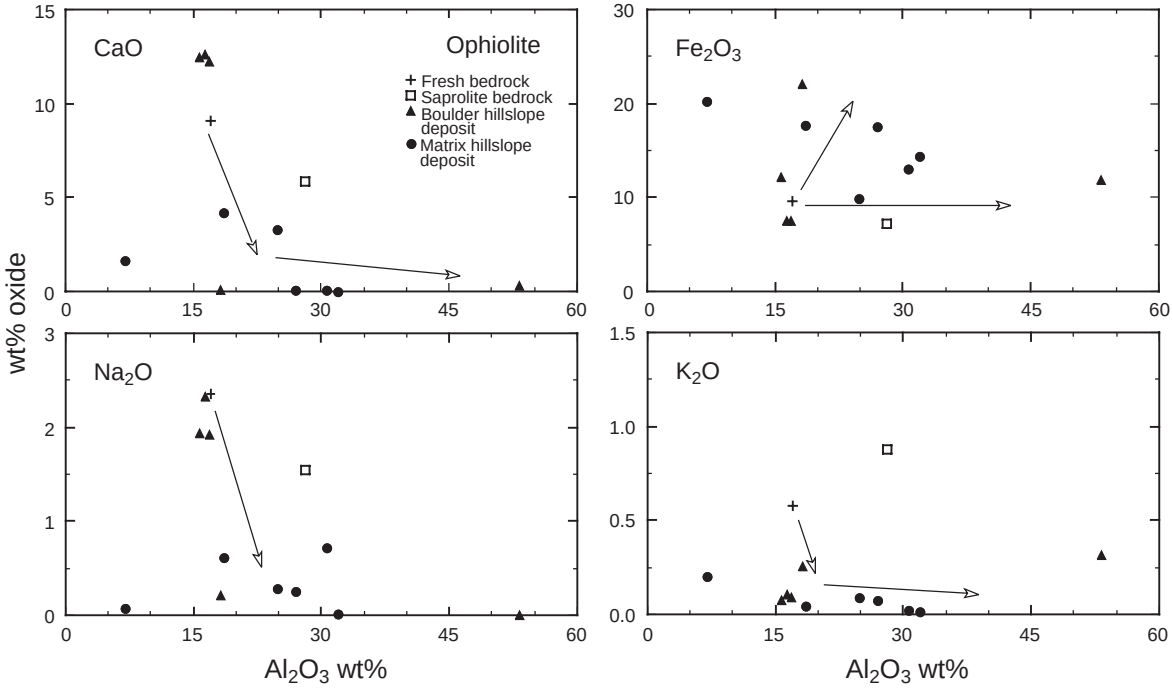

Fig. 4. Major element–Al_2O_3 variation diagrams (anhydrous basis) for samples derived from ophiolitic bedrock source.

Al_2O_3, with some scatter to high values. Fe_2O_3 contents show strong positive correlation with Al_2O_3, with values varying from 4.72 wt.% in fresh tonalite to almost 11 wt.% in the saprolites and matrix materials (Fig. 2). Mean values are around 8 wt.%. In contrast, Na_2O, CaO, and K_2O show weak negative correlation

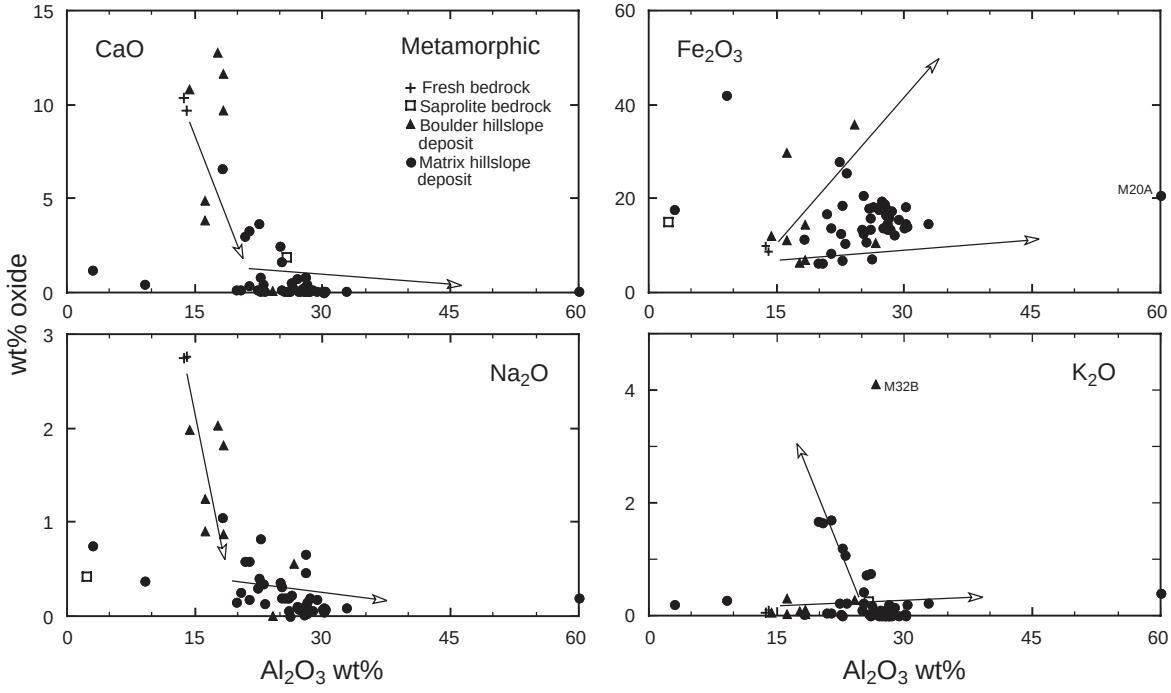

Fig. 5. Major element–Al_2O_3 variation diagrams (anhydrous basis) for samples derived from metamorphic bedrock source.

with Al_2O_3. Abundances of these elements in almost all saprolites and matrices are much lower than in the source material (Fig. 2), indicating substantial loss during weathering.

Material derived from volcanic–sedimentary sources shows consistent oxide trends comparable with those of the granitoid-derived samples (Fig. 3). Fresh basalt rock and boulder samples have higher CaO, Na_2O (Fig. 3), and MgO contents than the weathered materials. SiO_2, CaO, Na_2O, MgO and MnO display negative correlations with Al_2O_3, whereas TiO_2 and Fe_2O_3 are positively correlated. Al_2O_3 contents range from 14–18 wt.% in the source material to almost 30 wt.% in the weathering products. SiO_2 contents of the two volcanic source rocks differ considerably (49.62 and 61.51 wt.%). Most debris flow matrices have SiO_2 abundances between these values, despite their higher Al_2O_3 contents. Fe_2O_3 abundances range from a minimum of 6.4 wt.% in source basalt to almost 20% in the matrix. Both Fe_2O_3 and TiO_2 abundances reflect differing compositional controls depending on the dominance of volcanic versus sedimentary source material.

Samples derived from ophiolitic sources show almost no linear inter-oxide correlations, but in general trends are similar to those from granitic and volcanic–sedimentary sources (Fig. 4). Al_2O_3 values vary substantially, from 7 wt.% in a debris flow deposit to over 53 wt.% in a metagabbro; most matrix samples are more aluminous (25–32%) than the source rocks. SiO_2 abundances in all lithotypes are generally low and quite uniform (35–50 wt.%) irrespective of Al_2O_3 content. CaO, Na_2O, K_2O (Fig. 4) and MgO all tend to be depleted in the matrix samples compared to most of the source materials. In contrast, Fe_2O_3 contents in the matrices tend to be greater than those of metagabbro rock and boulders (Fig. 4). TiO_2 contents are variable (0.02–3.3 wt.% anhydrous) and show little systematic correlation with Al_2O_3 or lithotype (Table 1).

The oxide variation diagrams for the larger set of samples derived from metamorphic sources (Fig. 5) show Al_2O_3 contents of most source rocks and boulders fall in a relatively narrow range (15–20 wt.%). All except four of the analyzed matrix samples have higher values (21–40 wt.%), most significantly so. Although there is some scatter, the relationship between the source and matrix materials for the other major oxides is also clear. SiO_2 (not illustrated) contents of the source rocks are generally intermediate (40–56 wt.%), whereas the matrix samples have more variable abundances (mostly 31–62 wt.%). With a few exceptions, CaO, Na_2O (Fig. 5), and MgO are strongly depleted in the matrix samples compared to the both source rocks and boulders. TiO_2 (not illustrated) shows weak positive correlation with Al_2O_3, with values generally <2 wt.% in rock and boulder samples and 1–4 wt.% in the matrix. Fe_2O_3 contents of the host rocks and matrix also show positive correlation with Al_2O_3, with some boulder and matrix samples scattering to higher values (Fig. 5). In contrast to samples derived from granitoid and volcanic–sedimentary sources, K_2O contents of the metamorphic source rocks and most matrices are low (<0.5 wt.%). However, some matrix samples in the 20–30 wt.% Al_2O_3 range are slightly enriched (Fig. 5).

6. Evaluation of weathering trends

Degradation of feldspar and concomitant formation of clay minerals is the dominant process during chemical weathering of the upper crust. Calcium, sodium and potassium are generally removed from feldspars, increasing the proportion of alumina to alkalis in the weathered product (Nesbitt and Young, 1982).

The ternary A–CN–K system is useful for evaluating the compositions of fresh plagioclase- and K-feldspar-rich rocks and examining their weathering trends and their weathering products, the clay minerals (Nesbitt and Young, 1984, 1989; Fedo et al., 1995). The most intensely weathered samples plot highest on the diagram, reflecting preponderance of aluminous clay minerals. The slopes of predicted and observed trends lie subparallel to the A–CN boundary, because plagioclase is more susceptible to weathering than is K-feldspar, and hence Ca and Na are leached preferentially over K. Such trends intersect the A–K boundary once all plagioclase has been destroyed, and then trend toward the A apex because K is extracted from the residues in preference to Al.

Weathering trends for source rocks and slope deposits in the Aburrá Valley are shown in Fig. 6. Similar to the oxide diagrams, the samples are plotted by source lithology to compare the weathering trends from the source rock to the hillslope deposit material.

In general, the Aburrá Valley samples show similar trends to those described by Nesbitt and Young (1984, 1989). Rock samples and slightly weathered boulders plot near the feldspar join; moderately weathered samples, saprolite, and relatively unweathered matrix fall in the middle to upper part of the triangle, and most matrix samples, highly weathered boulder and saprolite horizons plot in the upper part. In general, all samples lie near the A–CN join. Granitoid-derived samples and those from volcanic–sedimentary sources are displaced a little toward the center of the triangle, reflecting their more felsic protolith, whereas metamorphic- and ophio-

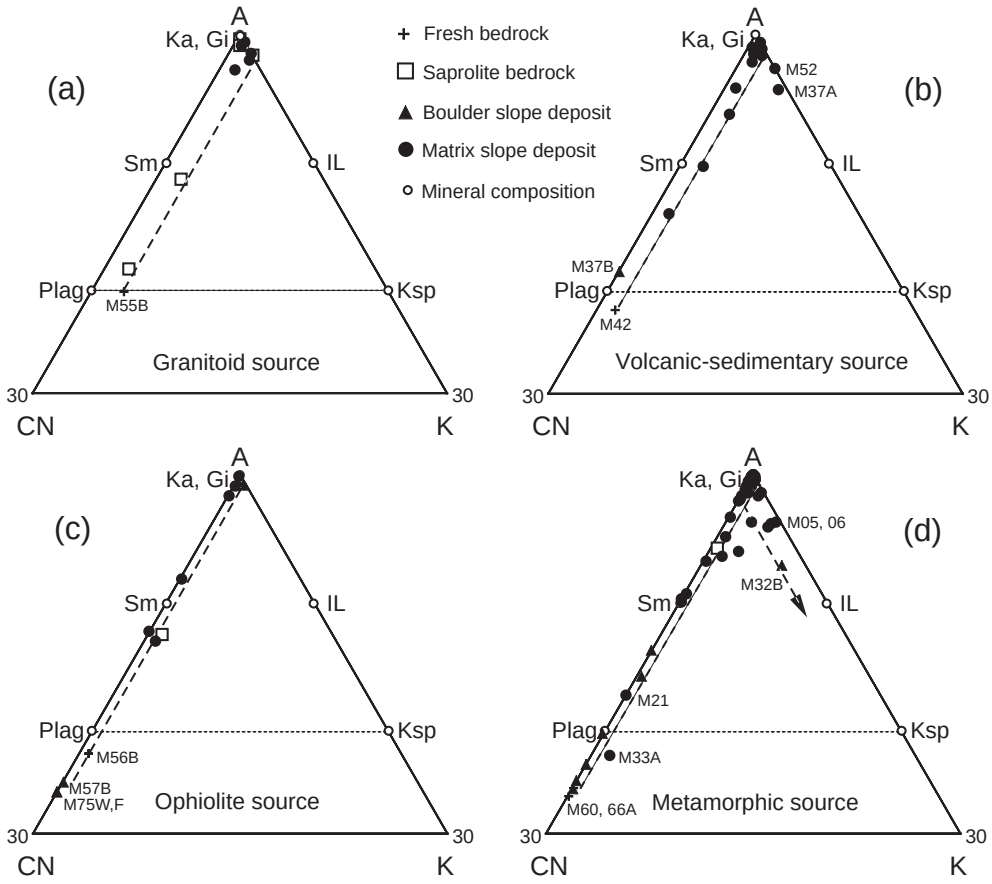

Fig. 6. A–CN–K diagrams illustrating the weathering trend of hillslope deposits and bedrock source of the Aburrá Valley, Colombia. (a) Granitoid bedrock source. (b) Volcanic–sedimentary bedrock source. (c) Ophiolitic bedrock source. (d) Metamorphic bedrock source. Dotted line Plag–Ksp represents the feldspar join. Dashed lines show weathering trends. Apices correspond to molecular proportions: A—Al_2O_3; CN—CaO*+Na_2O; K—K_2O. The CO_2 correction to derive CaO* was not applied in this study because CaO contents are generally very low and thus carbonate contents are minimal. Pl—plagioclase; Ksp—K-feldspar; Sm—smectite; IL—illite; Ka—kaolinite; Gi—gibbsite (Nesbitt and Young, 1984; 1989).

lite-derived samples generally plot along the A–CN edge.

The trend for the granitoid-derived samples lies subparallel to the A–CN join (Fig. 6a). The single fresh tonalite analyzed (M55B) plots on the feldspar join, indicating that feldspars are the dominant Al-bearing minerals in this rock. Positioning near the A–CN edge indicates a high proportion of plagioclase to K-feldspar. Analyzed saprolite samples from weathering profiles in the northern Aburrá Valley plot higher on the triangle, but track the general trend. Slope deposits matrices plot at the A apex, reflecting the preponderance of aluminous clay minerals within them. The weathering trend intercepts the A–K join, reflecting almost total destruction of plagioclase in the most weathered samples. From this point the weathering trend is deflected toward the A apex, reflecting loss of K in relation to Al.

Materials derived from volcanic–sedimentary sources show a trend similar to the granitoid-derived samples (Fig. 6b). Fresh basalt M42 and volcanic boulder M37B plot near the feldspar join and close to the A–CN edge, reflecting dominance of plagioclase. The middle of the weathering trend is formed by two matrix samples from alluviotorrential deposits, whereas slope deposit matrix samples plot near the A apex. Samples M37A and M52 are slightly enriched in K and plot close to the A–K join.

The ophiolitic samples lie almost on the A–CN edge (Fig. 6c). Rock (M56B) and fresh boulders (M57B, 75F, 75W) plot well below the feldspar join, reflecting the high initial abundances of CaO and Na_2O in these metagabbros (Table 1). The latter three boulders plot below the fresh rock, reflecting slight enrichment in CaO (+3.1–3.4 wt.%, Table 1) relative to the parent. Most matrix samples plot at the top of the triangle,

reflecting high concentrations of alumina-bearing minerals. A few matrix samples plot in a lower position near smectite composition, suggesting partial transformation of Ca and Na minerals to this clay mineral group. The weathering pattern is consistent to those described above, in which matrix samples have high alumina concentrations with respect to the fresh rock. The ophiolite trend does not intersect the A–K joint, reflecting very low initial values of K in the protolith.

Material derived from mainly amphibolitic metamorphic rocks in the northern Aburrá Valley, La Iguaná, and the southwestern valley show similar trends (Fig. 6d). Most samples lie along the A–CN boundary, but some scatter toward the A–K join, reflecting enrichment in K, possibly due to secondary illitization (Fedo et al., 1995). Rocks and fresh boulders from the metamorphic source plot well below the feldspar line, reflecting their mafic character and high initial values of CaO and Na_2O. Matrix samples M05 and M06 from the northern valley have relatively high K_2O contents (1.7 and 1.8 wt.% respectively). Both samples come from debris flows in which both metamorphic and granitic boulders are found, and hence have mixed sources, and thus higher initial K:CN ratios. Matrix samples M33A and M21 plot lower on the triangle than those from similar weathering grades. Both have anomalous MgO, CaO and Na_2O contents compared to other matrix samples, and their A–CN–K relations may thus have been disturbed by authigenic carbonate phases. Boulder sample M32B plots well toward the K apex, reflecting marked K enrichment (4.1 wt.%) and much lower CaO and Na_2O than most other samples of that type.

Because MgO and Fe_2O_3 are potentially mobile in tropical environments, it is essential to also evaluate the chemical behavior of these minerals in the weathering

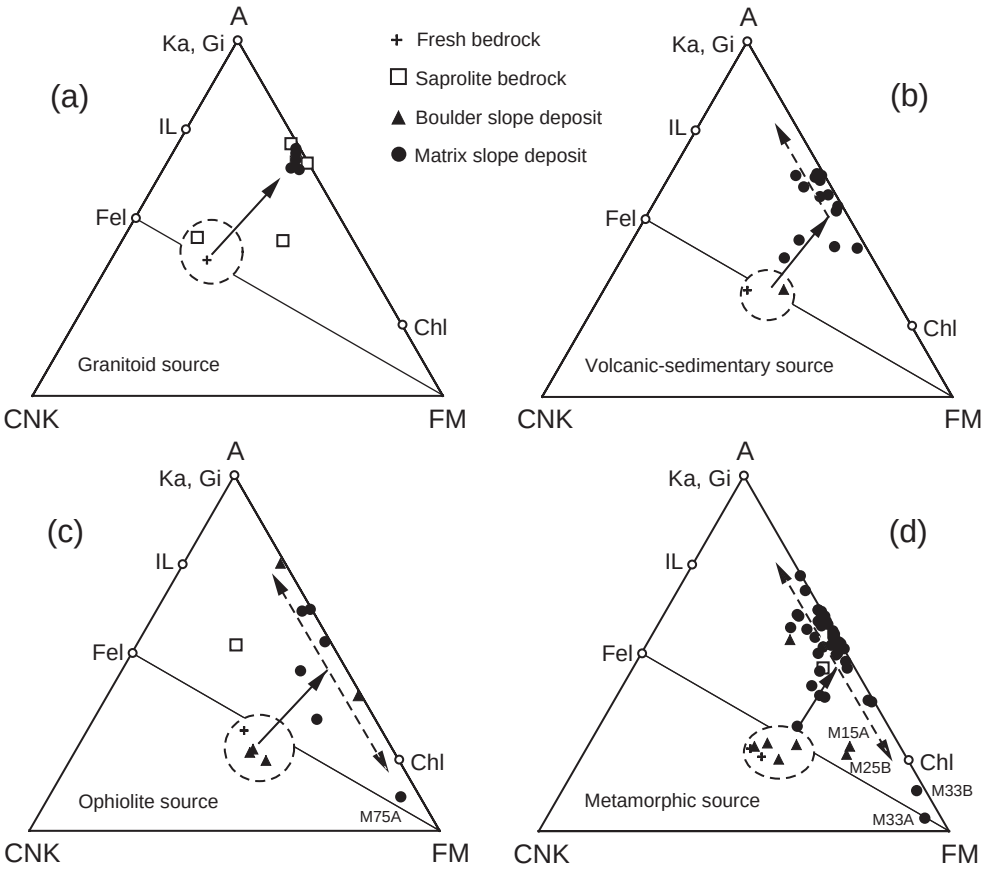

Fig. 7. A–CNK–FM diagrams illustrating the weathering trends of hillslope deposits and bedrock source in the Aburrá Valley, Colombia. (a) Granitoid bedrock source. (b) Volcanic–sedimentary bedrock source. (c) Ophiolitic bedrock source. (d) Metamorphic bedrock source. Line Fel–FM represents the feldspar–FM join. Solid arrows show the general trends as weathering increases. Dashed arrows represent subsequent depletion or enrichment from the general weathering trend. Dashed circles are the source composition. Apices correspond to molecular proportions, A—Al_2O_3; CNK—$CaO^*+Na_2O+K_2O$; FM—FeO^* (FeO total)+MgO. Fel—feldspar; Chl—chlorite; IL—illite; Ka—kaolinite; Gi—gibbsite (Nesbitt and Young, 1989; Nesbitt et al., 1996).

profiles. Nesbitt and Young (1989) introduced an A–CNK–FM diagram to illustrate the relationship between leucocratic and melanocratic constituents in weathering profiles.

A–CNK–FM diagrams for the four suites demonstrate the enrichment of MgO and Fe_2O_3 in the weathering profiles derived from metamorphic and ophiolitic sources (Fig. 7). The general tendency is for the fresh rocks and boulders to plot along the tieline between feldspar (Fel) and the FM apex, whereas matrix samples and saprolites are displaced toward the A–FM edge and the A apex.

Source provenance for the hillslope deposits is well reflected in the A–CNK–FM plots. Fresh tonalite plots on the upper part of the Fel–FM tieline, reflecting its relatively felsic composition. Volcanic–sedimentary source material lies lower along the Fel–FM tieline, but on the same trend, and ophiolite and metamorphic source materials lie a little closer to the FM apex (Fig. 7).

Matrix samples from granitic sources fall in a tight cluster on the A–FM join, reflecting dominance of aluminous clays (Fig. 7a). Volcanic-sourced material shows a similar trend (Fig. 7b). Matrix samples derived from sedimentary sources plot below this group, due to higher values of Fe_2O_3 and MgO. Samples derived from ophiolitic sources show considerable scatter, with displacement to high values of MgO and Fe_2O_3, and also to high values of Al_2O_3 (Fig. 7c). Metamorphic-sourced samples show more consistent trends (Fig 7d). In general, most matrix samples plot close to the FM apex. Fresh rocks and boulders fall slightly below the Fel–FM tieline, whereas matrix samples plot toward the A–FM edge. The weathering process forms a trend subparallel to the A–CNK edge, which then intercepts the A–FM join, and continues along that join toward the A apex.

The A–CNK–FM diagrams suggest that Fe and Mg play an important role in the weathering processes which affected the Aburrá Valley, especially in the material derived from ophiolitic and metamorphic sources. These elements do not display regular patterns as the intensity of weathering increases, suggesting that within these two groups both Fe and Mg may be highly mobile under some conditions. Samples which plot away from the general trend are those with exceptionally low Al_2O_3 contents and high Fe_2O_3 and MgO, such as M75A, M33A, M33B, M25B, and M15A (Fig. 7; Table 1).

7. Evaluation of weathering intensity

Nesbitt and Young (1982) suggested a good measure of the degree of weathering can be obtained by calculation of the Chemical Index of Alteration (CIA), based on molecular proportions:

$$\mathrm{CIA} = \mathrm{Al_2O_3} / (\mathrm{Al_2O_3} + \mathrm{CaO^*} + \mathrm{Na_2O} + \mathrm{K_2O}) \times 100$$

where CaO* is the amount of CaO incorporated in the silicate fraction of the rock. Assuming Al is immobile, changes in CIA reflect changes in the proportions of feldspar and the various clay minerals developed in the profiles. High CIA values reflect the removal of labile cations relative to stable residual constituents during weathering, and low CIA values indicate the near absence of chemical alteration (Nesbitt and Young, 1982). Chemical Index Alteration (CIA) values are directly represented on the A–CN–K triangle. The CIA corresponds to the horizontal projection on a vertical scale ranging from 0 (A–CN join) to 100 (A apex), where the fresh feldspar join has a value of 50. Fresh rocks and minerals ranging in composition from gabbro through to plagioclase and K-feldspar have similar CIA values of about 40 to 50, whereas completely weathered material has a CIA value of about 100 (Fedo et al., 1995).

All Aburrá Valley samples are plotted on a summary A–CN–K diagram in Fig. 8. In general, the rock samples yield values between 38 and 60, including some slightly weathered boulders in hillslope deposits. Saprolites, boulders, and moderately weathered matrix material have ratios of 62 to 85, whereas completely weathered matrix, saprolite, and boulder samples have values ranging from 85 to 100. Anomalous low values are given by samples enriched in Fe_2O_3, MgO, and depleted in Al_2O_3 (M75A, 33A, 33B, 33D), as well as samples enriched in CaO (M58, 75B). In general, however, the CIA ratios show a relatively orderly progression from low values in the source materials to very high values in the matrix materials.

Loss on ignition (LOI) is another important parameter that can be used to evaluate weathering intensity. Sueoka et al. (1985, in Irfan, 1999) proposed LOI as a good indicator of the degree of chemical weathering. We have also used LOI to evaluate the intensity of weathering in the Aburrá Valley, because it represents an independent and additional parameter.

In general, LOI increases as the intensity of weathering increases. LOI values vary from 1% in the rock samples to 19% in the matrix samples. Anomalous data were obtained for two boulder samples from the ophiolitic source, which had LOI of 30% and 28%. Loss on ignition is greater in matrix samples and boulders than in the fresh rocks.

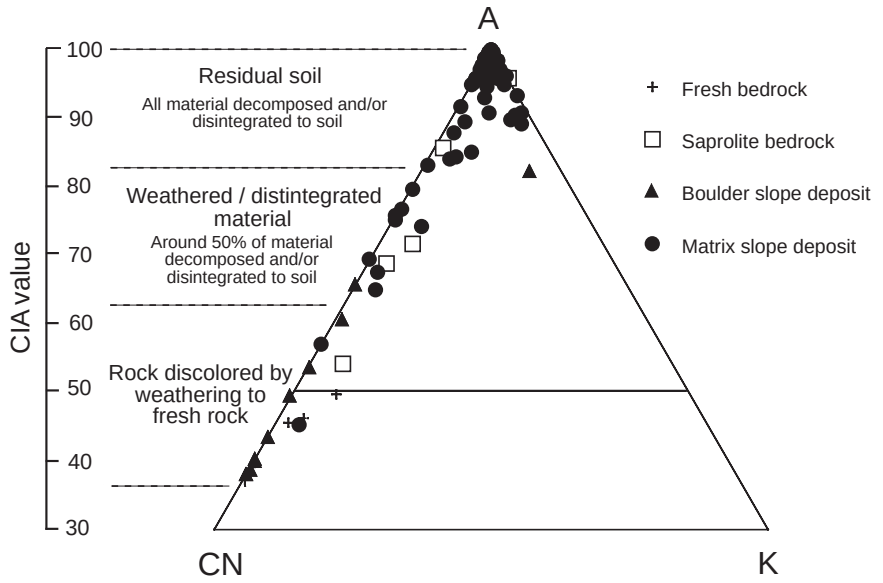

Fig. 8. A–CN–K diagram illustrating weathering intensity (CIA values) of all samples collected from hillslope deposits and bedrock source in the Aburrá Valley. The CIA scale is divided into the simplified typical weathering profile described by the Geological Society of London in Lambe (1996).

A reasonable relationship is seen between CIA and LOI (Fig. 9), with both increasing according to the grade of weathering. Rocks and fresh boulders cluster in the lower part, at LOI values of around 2–3% and CIA 40–50. Granitic source samples generally have lower LOI values, plotting below the general trend. Ophiolitic and metamorphic samples scatter to higher LOI values at high CIA. The general trend is variable for highly decomposed samples, especially for those derived from ophiolitic and metamorphic sources.

Irfan (1996) introduced the Mobiles index (Imob), another parameter useful for evaluating weathering intensity. This index is based on the extent of depletion of

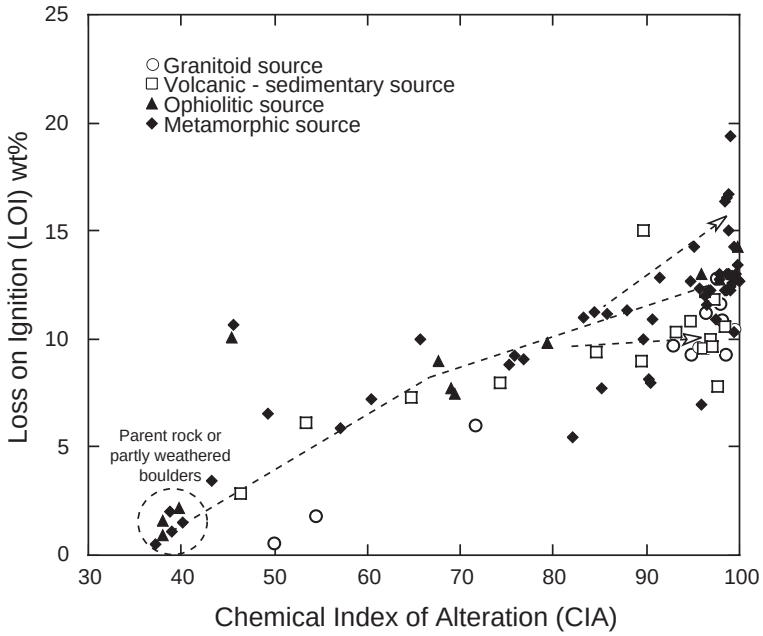

Fig. 9. Chemical Index of Alteration (CIA) versus loss on ignition (LOI) for all Aburrá Valley samples, differentiated by source lithotype. Dashed arrows show the general trend (fitted by eye) and the inflexion point at CIA ~ 65. Dashed circle shows the position of the parent rocks.

CaO, Na_2O, and K_2O between fresh parent rock and weathered product, namely:

$$\text{Mob} = (K_2O + Na_2O + CaO)\text{mole}$$

$$\text{Mobiles index (Imob)} = (\text{Mob}_{\text{fresh}} - \text{Mob}_{\text{weathered}}) / \text{Mob}_{\text{weathered}}$$

where $\text{Mob}_{\text{fresh}}$ and $\text{Mob}_{\text{weathered}}$ are the total (K_2O+Na_2O+CaO) contents in the fresh and weathered rock, respectively (Irfan, 1996). The Mobiles index is defined as a molecular ratio, in which the composition of weathered material is normalized against that of the parent rock, using the above equation. This index considers only the most mobile elements (K_2O, Na_2O, CaO), and provides valuable information because it combines data from both the weathering products and their fresh parent.

The Mobiles index serves as an index of the degree of decomposition of feldspar-bearing rocks, particularly under reasonably well-drained conditions (Irfan, 1996). Standard samples were used for each source lithology to calculate the Mobiles index along the Aburrá Valley. Sample M55B was used for the granitic source, M66A for the metamorphic source, M42 for the volcanic–sedimentary source, and M56B for the ophiolitic source material.

Fig. 10 shows the correlation between the Mobiles index and CIA; data are given in Table 1. Samples derived from granitic and volcano-sedimentary sources plot along a linear trend, at slightly higher values of CIA than the other sources. Samples from metamorphic and ophiolitic source materials form a discontinuous trend. The first part of this trend is linear and at lower CIA than in the granite and volcano-sedimentary groups, whereas the second part steepens at CIA ~60 and Imob 0.6, until CIA and Imob become equal for all suites.

Three ophiolite- and metamorphic-derived samples with unusually low Al_2O_3 and elevated MgO and Fe_2O_3 contents compared to other samples in those groups plot in the lower part, well away from the general trend (Fig. 10). This suggests that the Al_2O_3 contents and CIA ratios of these samples have been reduced, possibly through sesquioxide development, as discussed further below. However, the Mobiles index values of these samples are similar to most other ophiolitic and metamorphic weathering products. Because the Mobiles index does not utilize the abundances of Al_2O_3, Fe_2O_3 or MgO, the overall trend of the ophiolitic- and metamorphic-sourced suites can be used to estimate the original CIA values of these anomalous samples. This is done simply by vertical projection, with original CIA corresponding to the intersection with the main trend. The estimated CIA values vary from 87 to 94 (Fig. 10),

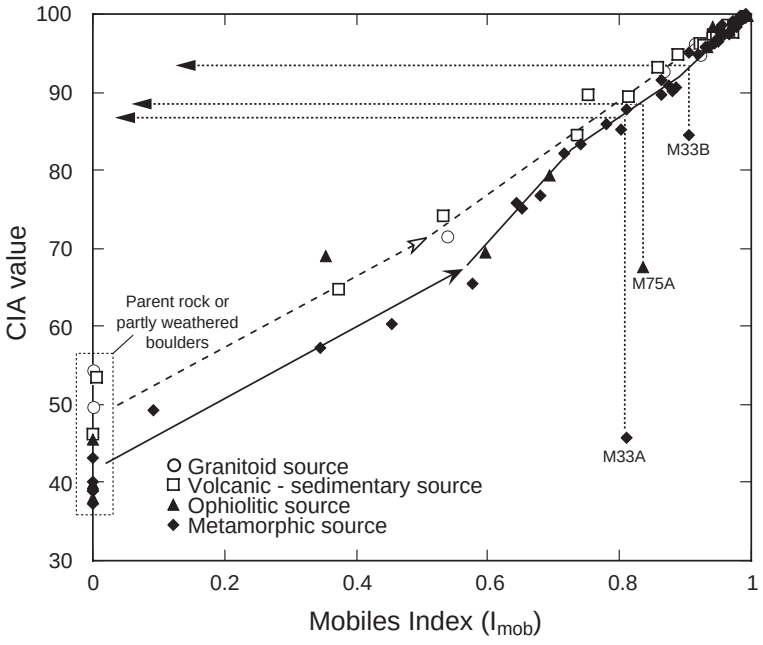

Fig. 10. Chemical Index of Alteration (CIA) versus Mobiles index (Imob). Solid arrow represents the general trend (fitted by eye) in the ophiolitic and metamorphic suite. Samples M33A, 75A, and 33B plot away from the trend, but projection to the general trend yields CIA values of 87–94 (dotted lines). Dashed arrow line is the trend for material derived from granitoid and volcanic–sedimentary sources.

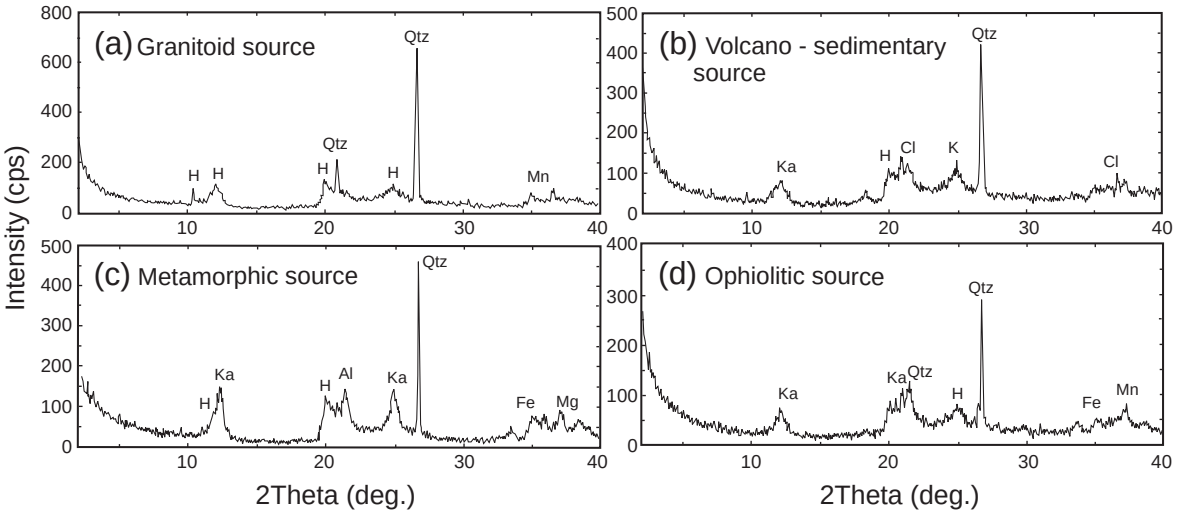

Fig. 11. Typical X-ray diffraction patterns of samples from hillslope deposits by bedrock source. (a) Granitoid source. (b) Volcano-sedimentary source. (c) Metamorphic source. (d) Ophiolitic source. Qtz—quartz; H—halloysite; Ka—kaolin; Cl—clinochrysotile; Al—aluminum hydroxide; Fe—ferrihydrite; Mg—magnesium oxide; Mn—manganese oxide.

suggesting advanced weathering for these samples, in accordance with their high LOI values.

8. Weathering product mineralogy

Example X-ray diffractograms of the hillslope deposits are given in Fig. 11. The mineralogy is dominated by quartz, kaolinite, and halloysite. Iron mineral peaks also occurred in all samples, but were most pronounced in samples derived from ophiolitic and metamorphic sources, indicating the presence of hematite and goethite produced by intensive tropical weathering. All samples analyzed contained magnesium and iron oxides. High contents of MgO, CaO, and Na_2O in samples M33D and M75B correspond to the presence of tremolite/actinolite and anorthite (Fig. 12a,c, respectively). High concentrations of MgO and depletion of Al_2O_3 in samples M33A and M75A are correlated with the presence of clinochlore and clinochrysotile. High concentrations of Fe_2O_3 in samples such as M33B are associated with significant peaks for hematite and goethite (Fig. 12b), whereas the high Al_2O_3 concentrations

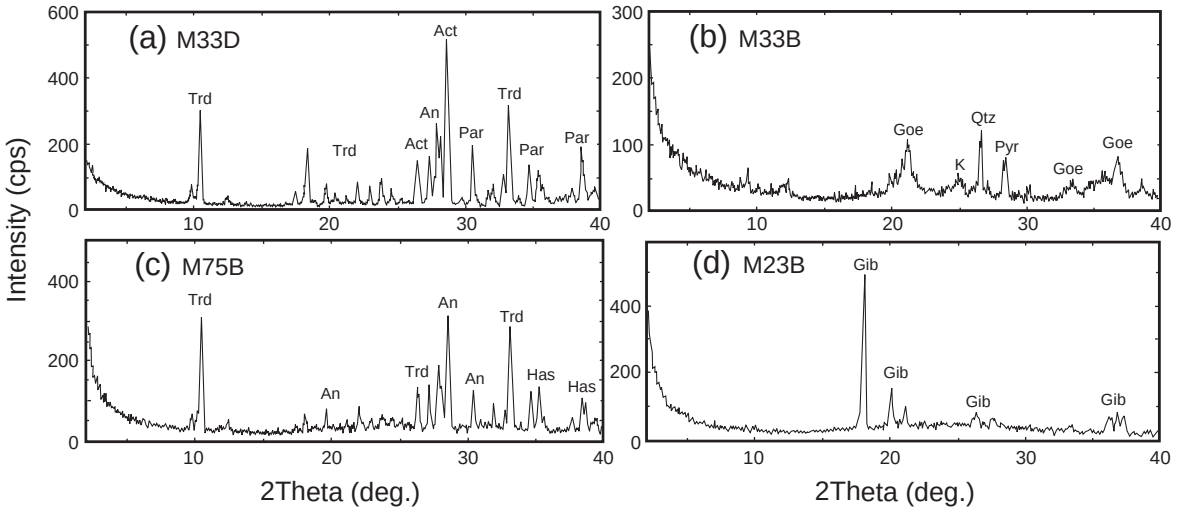

Fig. 12. X-ray diffraction patterns of samples enriched in sesquioxides. (a) Sample M33D, hillslope deposit boulder from metamorphic source. (b) Sample M33E, hillslope deposit matrix from metamorphic source. (c) Sample M75B, hillslope boulder from ophiolitic source. (d) Sample M23B, hillslope deposit boulder from ophiolitic source. Goe—goethite; Gib—gibbsite; Trd—tremolite; Act—actinolite; An—anorthite; Par—pargasite; Qtz—quartz; Pyr—pyrolusite; K—kaolin; Has—hastingsite.

seen in samples such as M23B reflect the presence of abundant gibbsite (Fig. 12d). Samples M23B and M24B, which have high LOI of 30.26% and 28.15% respectively, also have high gibbsite contents.

9. Discussion

The degree of weathering is one of the most significant factors controlling the type and abundance of clay minerals (Duzgoren-Aydin et al., 2002). Tropical weathering in the Aburrá Valley is characterized by the loss of CaO, Na_2O, and K_2O, and increase in Al_2O_3. Minerallogically, these chemical changes reflect the formation of secondary clay minerals, predominantly kaolin and halloysite. Halloysite is the first kaolin mineral produced, and this subsequently changes to kaolinite as the intensity of weathering increases (Irfan, 1996). Kaolinite is formed in the more advanced stages of weathering. Goethite and hematite are common in the weathered rocks and residual soils of the Aburrá Valley, and are often responsible for the yellowish and reddish colors of these tropical soils.

Scattering of the ophiolitic- and metamorphic-sourced samples on several of the plots used here suggests that the behavior of the elements involved is not only controlled by the intensity of weathering. This dispersion is probably associated with compositional variation in the metamorphic sequence parent, and by the mineralogical composition of the ophiolitic source. Considerable lithological variation has been reported from the metamorphic complex, such as layers of schists, amphibolites and gneisses interbedded over short distances (GSM, 2002). Such lithologic variations in the ophiolitic and metamorphic sources may be sensitive parameters in the weathering profile. Price and Velbel (2003) considered that segregation of micaceous minerals from tectosilicates and development of foliation during metamorphism produce layers with differing chemical and mineral compositions, and thus with different susceptibility to weathering. These conditions suggest that certain major oxides such as Al_2O_3, Fe_2O_3, and TiO_2 do not remain constant even though they are usually considered to be immobile.

Many authors have discussed the role of Fe and Mg in weathering analyses. Price and Velbel (2003) considered that iron concentrations are rather sensitive to redox conditions, which may not be consistent throughout the weathering profile. Consequently, iron abundances in weathering products may be controlled by modern or ancient groundwater levels rather than by the extent of weathering. Duzgoren-Aydin et al. (2002) considered that the effects of Fe and Mn oxides on the trends of chemical weathering are substantial. The geochemical behavior of oxides in weathered samples is modified, so as Fe and Mn oxide and hydroxide contents increase, samples contain less Al_2O_3, and significantly greater Fe_2O_3 and MgO contents.

Intensive tropical weathering is reflected in the formation of iron and aluminum sesquioxides. Strong sesquioxide enrichment is found in the northwestern and southeastern Aburrá Valley. This process, referred to as lateritization, characterizes the final stage of the weathering profiles developed in these areas. Laterites consist predominantly of mineral assemblages containing goethite, hematite, aluminium hydroxides, kaolinite minerals, and quartz (Schellmann, 1981). Some examples with granular or nodular appearance have clearly been affected by iron remobilization and reconcentration, and can be described as ferricretes (Voicu and Bardoux, 2002). Zones of rounded and subrounded nodules commonly occur between successive hillslope deposits within the Aburrá Valley. Such ferruginous nodules are formed by de-ferruginization of previously associated kaolinite and Fe oxyhydroxides; and can be interpreted as the result of groundwater fluctuation zones, reflecting change from previously wet to drier conditions (Irfan, 1996; Tonui et al., 2003).

The physical and engineering properties of soils can be greatly influenced by the presence of sesquioxides reducing the plasticity of the constituent materials (Irfan, 1996; Duzgoren-Aydin et al., 2002). Sesquioxides can physically cement adjacent grains, increasing cohesion, and reduce the ability of clay minerals to absorb water (Irfan, 1996).

Chemical weathering indices including CIA are greatly influenced by the presence of sesquioxides of iron and aluminum (goethite, hematite, and gibbsite) when these occur in significant quantities, such as in samples M33B, 20A–C, 23B, and 24B. All of these samples are characterized by anomalously high LOI. Sesquioxides lose their water of hydration when dried over 105 °C (Irfan, 1996), so this water is reflected in our LOI determinations. In addition, samples enriched in iron sesquioxides have lower CIA values, and have different enrichment trends on the A–CNK–FM diagrams. The Mobiles index correlates well with the intensity of weathering due to normalization of the weathered material against the parent rock, and it does not include Fe and Al. The Mobiles index provides a good measure for adjusting sesquioxide-enriched samples to the normal trend, thus providing a proper chemical weathering index for such samples.

The correlation between CIA, LOI, and Imob yields consistent results. These trends reveal a break around a

CIA ratio of 65, and both CIA/Imob and CIA/LOI ratios increase at this value. This break could represent a marked boundary between weathered rock and residual soil, characterized by a significant increase in the contents of secondary clay minerals and relatively large isovolumetric chemical changes (Voicu and Bardoux, 2002). Although geochemical changes are significant even during the early stages of weathering, formation of secondary minerals is accelerated in the later stages. This weathering sequence is observed in the diagrams employed here.

The results from the Aburrá Valley show that high tropical rainfall combined with humid climatic conditions has favored weathering of the bedrock to considerable depth, and to varying degree. The intensive weathering recorded in the valley reflects dominantly warm and humid conditions, which persisted for a long time. Prolonged high rainfall is suggested because the soils are extensively leached and cation-depleted phases such as gibbsite, kaolinite, and halloysite are formed (Irfan, 1996; Johnsson et al., 1993; Duzgoren-Aydin et al., 2002). Furthermore, soils dominated by kaolinite are developed on older geomorphic surfaces, and are more leached than those from younger parts of the landscape (Johnsson et al., 1993).

Intensive warm and humid conditions could thus be responsible for the weathering and mobilization of large and old hillslope deposits in the Aburrá Valley during the Quaternary. These processes, triggered by saturation of upslope regolith, suggest humid environmental conditions with sufficient water to promote weathering and to initiate debris flows. However, in addition to the influence of climatic factors, slope evolution of the Aburrá Valley has also undoubtedly been influenced by tectonism. Morphological evidence such as presence of large boulders and the sheer volume of hillslope deposits suggest influence of seismicity in the generation of these mass movements, as suggested in previous work characterizing the recent tectonic history of the Aburrá Valley (GSM, 1999, 2002; Rendón, 2003; Yokota and Ortiz, 2003). The cumulative effects of many low-magnitude seismic events, steep slopes, and thick weathering profiles are also important factors in slope instability, in addition to the intense weathering observed in this study.

10. Conclusions

Chemical weathering study of parent rocks and hillslope deposits in the Aburrá Valley, Colombia, was undertaken to identify weathering trends and intensity, and to examine the relationships between source material and hillslope sediments. The material composing the valley slopes displays an intense weathering history. Weathering is characterized by increased development of clay minerals and sesquioxides. Concentrations of CaO, Na_2O, K_2O decrease markedly in the weathering products compared to the fresh source rocks, regardless of lithotype, whereas concentrations of Al_2O_3, Fe_2O_3, and MgO increase significantly. Kaolinite and halloysite are the dominant clay mineral in the most intensely weathered material.

Weathering trends from granitoid, volcanic–sedimentary, ophiolite, and metamorphic sources are linear in A–CN–K space, and follow the trends predicted by Nesbitt and Young (1984), validating the correlation established between the hillslope deposits and their various parents.

Chemical weathering indices provide a good indication of the degree of weathering in the hillslope deposit and bedrock source of the Aburrá Valley. LOI and CIA values increase with increasing weathering grade. However, these indices are very sensitive to sesquioxide contents, yielding anomalous weathering indices for lateritic horizons. Consequently they should be used carefully, especially in weathering profiles developed under intensive tropical conditions, where lateritization produces significant quantities of sesquioxides. Mobile index (Imob) values are more consistent, changing systematically as weathering intensity increases. Differing chemical indices thus should be combined to obtain best results, especially if the selected indices are based on different criteria. The combination of LOI, CIA, and Imob used here suggests weathering in the Aburrá Valley was prolonged and intense.

Acknowledgements

This project was financially supported by a Japan–Inter-American Development Bank (IDB) scholarship to the first author. We are also grateful to Yoshihiro Sawada for the access to the XRF; to the Soil Laboratory of the Universidad Nacional de Colombia, Facultad de Minas, Medellín for the use of their facilities for initial sample preparation; and to our reviewers for their very helpful comments.

References

Arel, E., Tugrul, A., 2001. Weathering and its relation to geomechanical properties of Cavusbasi granitic rocks in northwestern Turkey. Bull. Eng. Geol. Environ. 60, 123–133.

Cooper, M.A., Addison, F.T., Alvarez, R., Coral, M., Graham, R.H., Hayward, A.B., Howe, S., Martinez, J., Naar, J., Peñas, R., Pulham, A.J., Taborda, A., 1995. Basin development and tectonic history of

the Llano Basin, Eastern Cordillera, and middle Magdalena Valley, Colombia. Am. Assoc. Petrol. Geol. Bull. 79, 1421–1443.

Duzgoren-Aydin, N.S., Aydin, A., Malpas, J., 2002. Distribution of clay minerals along a weathered pyroclastic profile, Hong Kong. Catena 50, 17–41.

Ego, F., Sebrier, M., 1995. Is the Cauca–Patia and Romeral fault system left- or right-lateral? Geophys. Res. Lett. 22, 33–36.

Fedo, C.M., Nesbitt, H.W., Young, G.M., 1995. Unraveling the effects of potassium metasomatism in sedimentary rocks and paleosols, with implications for paleoweathering conditions and provenance. Geology 23, 921–924.

GSM—Grupo de Sismología de Medellín, 1999. Instrumentación y microzonificación sísmica del área urbana de Medellín. Municipio de Medellín—Sistema Municipal de Prevención y Atención de Desastres, 135 pp.

GSM—Grupo de Sismología de Medellín, 2002. Microzonificación sísmica de los municipios del Valle de Aburrá y definición de zonas de riesgo por movimientos en masa e inundaciones. Area Metropolitana del Valle de Aburrá, Internal report, Chapter 3: Geología del Valle de Aburrá, 76 pp.

Gupta, A., Rao, K., 2001. Weathering indices and their applicability for crystalline rocks. Bull. Eng. Geol. Environ. 60, 201–221.

Irfan, T.Y., 1996. Mineralogy, fabric properties and classification of weathered granites in Hong Kong. Q. J. Eng. Geol. 29, 5–35.

Irfan, T.Y., 1999. Characterization of weathered volcanic rocks in Hong Kong. Q. J. Eng. Geol. 32, 317–348.

Johnsson, M.J., Ellen, S.D., Mckittrick, M.A., 1993. Intensity and duration of chemical weathering: an example from soil clays of the southeastern Koolau Mountains, Oahu, Hawaii. In: Johnsson, M.J., Basu, A. (Eds.), Processes controlling the composition of clastic sediments, Geol. Soc. Amer. Spec. Paper, vol. 284, pp. 147–170.

Kerr, A.C., Tarney, J., Marriner, G.F., Nivia, A., Saunders, A.D., Klaver, G.Th., 1996. The geochemistry and tectonic setting of Late Cretaceous Caribbean and Colombian volcanism. J. South Am. Earth Sci. 9, 111–120.

Kimura, J.-I., Yamada, Y., 1996. Evaluation of major and trace element analyses using a flux to sample ratio of two to one glass beads. J. Mineral. Petrol. Econ. Geol. 91, 62–72.

Lambe, P., 1996. Residual soils. Landslides: investigation and mitigation. In: Turner, K., Schuster, R. (Eds.), Landslides Investigation and Mitigation, Special Report,. Transportation Research Board, National Research Council, vol. 247, pp. 507–524.

Maya, M., Gonzalez, H., 1995. Unidades litodémicas en la Cordillera Central de Colombia. Bol. Geol. Inst. Investig. Geocienc., Miner. Qum. Ingeominas 35, 43–57.

McCourt, W., Aspden, J., Brook, M., 1984. New geological and geochronological data from the Colombian Andes: continental growth by multiple accretion. J. Geol. Soc. 141, 831–845.

McFadden, L., 1988. Climatic influences on rates and processes of soil development in Quaternary deposits of southern California. Spec. Pap.-Geol. Soc. Am. 216, 153–177.

Modenesi-Gauttieri, M.C., de Toledo, M.C.M., 1996. Weathering and the formation of hillslope deposits in tropical highlands of Itatiaia–southeastern Brazil. Catena 27, 81–103.

Moon, V., Jayawardane, J., 2004. Geomechanical and geochemical changes during early stages of weathering of Karamu Basalt, New Zealand. Eng. Geol. 74, 57–72.

Nesbitt, H.W., Young, G.M., 1982. Early Proterozoic climates and plate motions inferred from major element chemistry of lutites. Nature 279, 715–717.

Nesbitt, H.W., Young, G.M., 1984. Prediction of some weathering trends of plutonic and volcanic rocks based on thermodynamic and kinetic considerations. Geochim. Cosmochim. Acta 48, 1523–1534.

Nesbitt, H.W., Young, G.M., 1989. Formation and diagenesis of weathering profiles. J. Geol. 97, 129–147.

Nesbitt, H.W., Young, G.M., McLennan, S.M., Keays, R.R., 1996. Effects of chemical weathering and sorting on the petrogenesis of siliciclastic sediments, with implication for provenance studies. J. Geol. 104, 525–542.

Ng, C.W., Guan, P., Shang, Y.J., 2001. Weathering mechanisms and indices of the igneous rocks of Hong Kong. Q. J. Eng. Geol. 34, 133–151.

PNUD-Proyecto de las Naciones Unidas para el Desarrollo-, Municipio de Medellín, 1995. Levantamiento integrado de cuencas hidrográficas del Municipio de Medellín. Departamento Administrativo de Planeación Metropolitana- Instituto MI RIO, 110 pp.

Price, J.R., Velbel, M.A., 2003. Chemical weathering indices applied to weathering profiles developed on heterogeneous felsic metamorphic parent rocks. Chem. Geol. 202, 397–416.

Rahardjo, H., Aung, K.K., Leong, E.C., Rezaur, R.B., 2004. Characteristics of residual soils in Singapore formed by weathering. Eng. Geol. 73, 157–169.

Rendón, D.A., 2003, Tectonic and sedimentary evolution of the upper Aburrá Valley, northern Colombian Andes, Unpublished MS thesis, Shimane University, 135 pp.

Restrepo, J.J., 1991. Datación de algunas cenizas volcánicas de Antioquia por el modo de trazas de fisión. AGID Rep. 16, 149–157.

Restrepo, J.J., Toussaint, J.F., 1984. Unidades Litológicas de los alrededores de Medellín. Mem Primera Conf Riesgo Geol. V. de A., Medellín, 20 pp.

Roser, B.P., Sawada, Y., Kabeto, K., 1998. Crushing performance and contamination trials of a tungsten carbide ring mill compared to agate grinding. Geosci. Rep. Shimane Univ. 17, 1–11.

Schellmann, W., 1981. Considerations on the definition and classification of laterites. Cited in: Bourman, R., Ollier, C.D., 2002. A critique of the Schellmann definition and classification of laterite. Catena 47, 117–131.

Sueoka, T., Lee, I.K., Huramatsu, M., Imamura, S., 1985. Geomechanical properties and engineering classification for decomposed granite soils in Kaduna district, Nigeria. Proc. First Int. Conf. Geomechanics in Tropical Lateritic and Saprolitic Soils, Brasilia, vol. 1, pp. 175–186.

Tonui, E., Eggleton, T., Taylor, G., 2003. Micromorphology and chemical weathering of K-rich trachyandesite and an associated sedimentary cover (Parkes SE Australia). Catena 53, 1–27.

Voicu, G., Bardoux, M., 2002. Geochemical behavior under tropical weathering of the Barama–Mazaruni greenstone belt at Omai gold mine, Guiana shield. Appl. Geochem. 17, 321–336.

Yokota, S., Iwamatsu, A., 1999. Weathering distribution in a steep slope of soft pyroclastic rocks as an indicator of slope instability. Eng. Geol. 55, 57–68.

Yokota, S., Ortiz, E., 2003. ^{14}C dating of an organic paleosol covering gravel beds distributed along the San Jerónimo Fault, Western Medellín, Colombia. Geosci. Rep. Shimane Univ. 22, 179–182.